

CHAPTER ONE HUNDRED FIFTY EIGHT

A NUMERICAL HINDCAST OF STORM CURRENTS ON THE NORWEGIAN SHELF

Cortis K. Cooper, A. M. ASCE*

INTRODUCTION

Objectives and Tasks

This paper describes an initial effort to model storm-driven currents and surge in the region indicated in Figure 1. The model results ultimately will be used in the design and operation of offshore oil platforms in the region.

The study consisted of four major tasks: 1) review of the data base and selection of the hindcast storms, 2) hindcast of the selected storms, 3) set-up and testing of the current model, and 4) hindcast of currents for the selected storms.

Description of Study Area

Current data were obtained from sites shown as solid circles in Figure 1. Each site consisted of an array of at least four Aanderaa current meters. Meters were typically placed at 50, 100, and 150 m below still water level, and at a few meters above the bottom.

Topographic effects play a major role in the shelf dynamics of the region. The Norwegian Trench is a dominant bathymetric feature with a characteristic depth of 300 m. Its outer edges are indicated by the dashed line in Figure 1. To the west of the trench, lies the Møre Plateau, a flat plane with an average depth of 150 m.

The worst storm conditions occur between late fall and early spring when the water column is generally well mixed. The region intersects the primary wintertime cyclone path and lies close to the average position of the polar front. Hence storms occur almost continuously during the winter season. Major storms in the region are extratropical, lasting for days. The region is too far south to be affected by the "polar low".

The frictional influence on shelf dynamics is relatively small, thus currents exhibit a strong inertial response (50 cm/s) during many storms. Within 50 km of the coast the response is affected by storm-induced alongshore pressure gradients.

The Norwegian Coastal Current is an important flow feature in the area. It flows from south to north through the Trench with a mean speed of 30 cm/s. However, the mean is occasionally interrupted by strongly baroclinic shelf waves which can generate surface currents of 150 cm/s (15).

*Petroleum Research and Development, Conoco Inc., Ponca City, OK 74603.

Tidal currents are primarily semidiurnal and of order 40 cm/s in magnitude. The banks and submarine canyons are known to affect currents, sometime dramatically in the form of splitting and vortex shedding (12).

Preview

The next section briefly describes the model formulation. Readers interested in more details should refer to Cooper and Pearce (9,10).

The third section describes the initial application of the model. During this phase of the study it was found that the model solution was dominated by a strong seiche. The seiche was caused by the reflective boundary conditions used in the initial grid system.

Following the difficulty with the boundary conditions, a review of existing techniques for specifying boundary conditions was performed and this is summarized in the fourth section. Readers should find this of general interest since a synthesis is absent in existing literature.

The fifth section describes the final grid system including a brief discussion of model sensitivity, and the sixth section presents some results from the storm hindcast, and discusses some of the reasons for the observed discrepancies between the model and data. The final section summarizes the previous sections, and describes the efforts presently underway to improve these efforts.

MODEL FORMULATION

The model is based on the primitive barotropic equations. The form on which they are applied in this application is numerically similar to the shallow water wave equations.

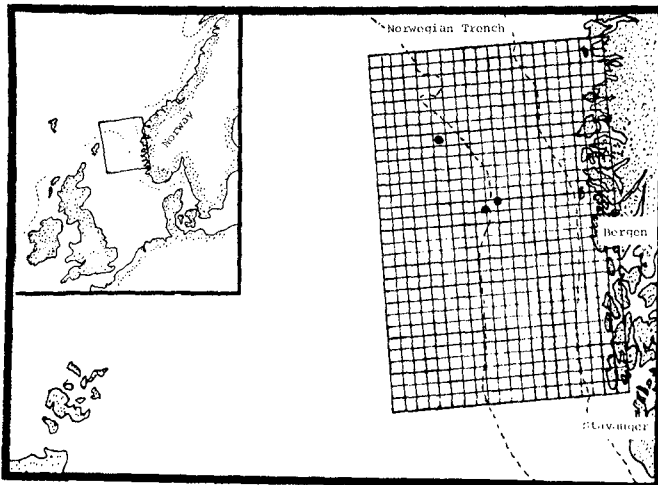


Figure 1: Model grid used in initial runs. Element size is 15.7 km.

Governing Equations

The model uses the linearized momentum equations:

$$0 = \frac{\partial u}{\partial t} + \frac{\rho_s}{\rho} g \frac{\partial \eta}{\partial x} - N_h (\nabla^2 u) - \frac{\partial}{\partial z} \left(N_v \frac{\partial u}{\partial z} \right) - fv + \frac{1}{\rho} \frac{\partial P_a}{\partial x} + \frac{g}{\rho} \int_0^z \frac{\partial \rho}{\partial x} d\xi,$$

$$0 = \frac{\partial v}{\partial t} + \frac{\rho_s}{\rho} g \frac{\partial \eta}{\partial y} - N_h (\nabla^2 v) - \frac{\partial}{\partial z} \left(N_v \frac{\partial v}{\partial z} \right) + fu + \frac{1}{\rho} \frac{\partial P_a}{\partial y} + \frac{g}{\rho} \int_0^z \frac{\partial \rho}{\partial y} d\xi,$$

where the symbols are defined as follows:

- t the time variable
- x, y the horizontal coordinates in a right-handed Cartesian coordinate system
- z the vertical coordinate, measured as positive downward from SWL
- u, v the horizontal velocity components in the x and y directions, respectively
- ρ_s the density of the fluid, where the s subscript indicates the value at the surface
- g the gravitational constant (9.8 m/s)
- η the water height of the free surface above SWL
- N_h the horizontal eddy-viscosity coefficient
- N_v the vertical eddy-viscosity coefficient
- f the Coriolis parameter $[-2\omega \sin \phi]$ where ω is the angular velocity of the earth and ϕ the latitude
- P_a the atmospheric pressure
- ∇^2 the Laplacian operator $\left[= \frac{\partial^2}{\partial x^2} + \frac{\partial^2}{\partial y^2} \right]$.

Note that the vertical velocity is assumed negligible. The density-gradient term was neglected in this application since adequate hydrographic data was unavailable.

The other governing equation used in the model is the continuity equation

$$\frac{\partial U}{\partial x} + \frac{\partial V}{\partial y} = \frac{\partial \eta}{\partial t},$$

where

U and V are the mass fluxes per unit length in the x and y directions, respectively.

Boundary Conditions

The boundary conditions at the surface are

$$\tau_{sx} = \left[-\rho N_v \frac{\partial u}{\partial z} \right] \Bigg|_{z=0}, \quad \tau_{sy} = \left[-\rho N_v \frac{\partial v}{\partial z} \right] \Bigg|_{z=0},$$

where τ_{sx} and τ_{sy} are the specified shear stresses at the surface in the x and y directions, respectively.

At the bottom a linearized friction law is used

$$\tau_{bx} = [\rho c_b u] \Big|_{z=H}, \quad \tau_{by} = [\rho c_b v] \Big|_{z=H},$$

where τ_{bx} and τ_{by} are the bottom shear stresses and c_b is a drag coefficient.

There were insufficient observations to provide boundary conditions on the horizontal boundaries so assumptions had to be made. Initially it was assumed that

- the mass fluxes perpendicular to the coastline were zero;
- the alongshore surface gradient on the cross-shelf boundaries was zero
- the amplitude at the open ocean boundaries was the barometric water rise (i.e. the inverted barometer effect).

Numerical Solution Technique

The governing equations and boundary conditions are transformed using the Galerkin technique. A cosine is used as the basis function in this model. The technique explicitly eliminates z from the transformed equations and greatly simplifies the eventual solution process. The dependence of u and v on z is implicitly retained in the final equations and the u and v velocity profiles can be regained whenever desired. A summary of the transformation is given in Cooper and Pearce (9). The method was originally suggested by Heaps (17) and has been used by others (11).

The transformed equations are solved on a staggered finite difference grid system using a "leap-frog" explicit scheme attributed to Lilly (21).

The horizontal grid used in the initial model consisted of 30 X 20 elements of 15.7 km each as shown in Figure 1. The grid was a compromise between the resolution needed to model the steep topographic features in the region, and the long integration times needed to model the regional storms. A more extensive grid was considered but the additional expense was not felt justified given the preliminary nature of the study.

INITIAL APPLICATION

Model Setup

The model uses three empirical coefficients to parameterize turbulent processes: bottom friction, vertical eddy viscosity, and lateral eddy viscosity. Values for these coefficients were based on equations available in the literature.

The bottom friction coefficient was derived using a Manning's coefficient for "straight and uniform earth". This suggests a value for the model coefficient of roughly 0.2 cm/s.

The vertical eddy viscosity is typically the most influential parameter for relatively deep water areas such as the Norwegian coast. Estimates in the literature for N_V vary by several orders of magnitude, but many of these estimates can be quickly discarded because of poor quality. Cooper and Pearce (9) successfully used a relationship suggested by Townsend (30) in their application in relatively shallow water. Ramming and Kowalik (25) offer a similar expression for shallow water which gives a value of about one-half that suggested by (30). Both expressions are proportional to the water depth—a reasonable assumption for shallow water. However, as one moves into deeper water it can be soundly argued that N_V reaches an upper limit which is totally dependent on the primary energy source - in this case wind. Ramming and Kowalik (25) suggest the upper bound for N_V is given by:

$$N_V = 4.7 \times 10^{-4} W^2/f$$

where W is the wind speed.

Substituting reasonable values for the Norwegian shelf gives $N_V = 40 \text{ cm}^2/\text{s}$ for a 10 m/s wind. The good experience with the Townsend relationship (30) suggests the doubling of the constant is in order, giving $N_V = 80$ - the value used for these initial runs.

The model can include a vertical variation in the eddy viscosity, and this is particularly useful in the case of stratified oceans. There are also physical arguments which suggest the viscosity should vary in the vicinity of a sheared surface. For this application the viscosity was kept constant in the vertical because stratification was negligible during the storms of interest, and because field data has not yet resolved the variation of viscosity near the sea surface.

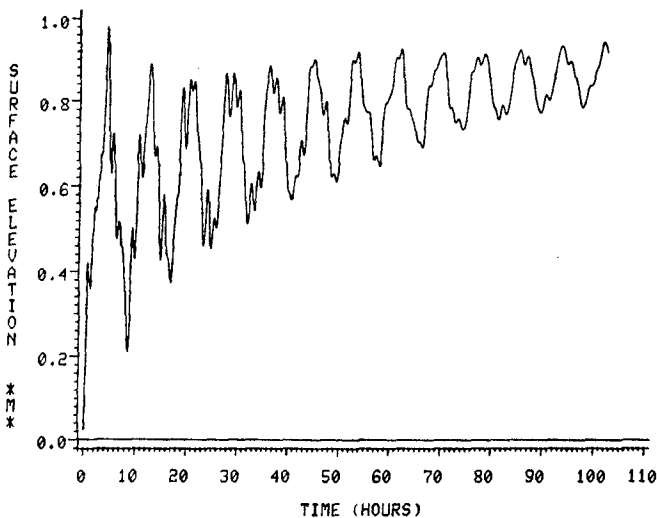


Figure 2: Modeled time series of surface elevation at the coast for initial model grid.

The horizontal eddy viscosity is primarily needed to account for subgrid turbulence, and advective terms. Previous experience by other modelers suggest a value on the order of $10^8 \text{ cm}^2/\text{s}$ (29).

Since there were inadequate observations along the boundary, it was necessary to make some assumptions. Initially the conditions were specified as described in the previous section. Similar boundary conditions have been used in many shallow water current and surge models.

The model was forced with a spatially constant wind blowing from the south. Wind speed was ramped in time; that is it was increased from zero at model start-up to 10 m/s at 20 hours. No tidal forcing was included.

Model Results

Figure 2 summarizes the essential result from the early model runs. The figure shows a time series of surface elevation at a coastal location. An oscillation with a well defined period of 5.5 hours is evident.

The oscillation in the figure corresponds to the seiche period or fundamental free wave mode of the basin in the cross-shelf direction. This is easily shown by substituting the characteristic dimensions of the model basin into the analytic solution given in Lamb (19). Note that the open boundary is a node, and hence the analytic solution in (19) must be doubled.

The seiche is a numerical aberration which results from the ocean boundary conditions. These conditions reflect all incident wave energy (26). Hence, when the wind first starts, it generates free gravity waves within the model domain. These waves eventually impact the ocean boundaries and are reflected back into the model domain. The reflected waves serve to further excite the basin because their frequency is the fundamental mode.

It is clear from these results that a further refinement of the ocean boundary conditions is needed. Some of the alternatives are reviewed in the following section.

OVERVIEW OF HORIZONTAL BOUNDARY CONDITIONS

Having adequate data along the outer boundary of a geophysical fluids model is as rare as the proverbial hen's tooth. Thus assumptions must be made. A review of the literature revealed five types of boundary conditions which have been used in shallow water wave models: 1) variable specification, 2) telescoping, nested or stretched grids, 3) energy absorbing elements, 4) Sommerfeld radiation condition, and 5) free/forced wave modes.

Each of these is summarized below including: a description of the method, examples of previous applications, advantages, and disadvantages. It should be kept in mind that the discussion applies only to the shallow water wave equations.

Variable Specification

In this technique, one or more of the dependent variables are specified on the boundary. For the initial runs described above, η on the cross-shelf boundary is set to η at the internal element normal to the boundary at each

time step. In other words a one-sided spatial difference across one element is used. On the alongshore boundary, η is set to the inverted barometric rise - in essence a specified constant.

Variable specification has dominated surge modeling. For instance Beardsley and Haidvogel (1) specified η equal to the inverted barometer effect along all ocean boundaries. Forristall et al. (13) specified the flow normal to the boundary equal to zero on the alongshore boundary, and the gradient of the flow equal to zero on the cross-shelf boundaries.

The major advantage of this approach is that it is simple to implement in the code of a numerical model. In addition, the conditions perform reasonably well for forced steady-state flows such as Ekman transport because they will allow realistic alongshore pressure gradients to develop.

The major disadvantage of the approach is that it reflects incident waves. In the case of one-sided spatial differences or constants such as used in this model, the condition is totally reflective as concisely demonstrated by Reid (26).

Fortunately, for many applications reflections are not important. For example, in the case of storm surge models, the grid systems are in predominately shallow water. Two factors work in favor of the modeler: 1) the system is frictionally dominated so reflections are rapidly dampened, and 2) the travel time of long waves is large relative to the model integration time so reflections do not have time to hit the boundary and return to the coast (the primary area of interest). Reflections are also not a problem in quasi-steady or steady-state problems such as (10). Unfortunately, none of these factors apply for the Norwegian Shelf Model. In other words, the system is not frictionally dominated, nor is the integration time short. Furthermore, transient conditions are of major interest.

Telescoping, Nested and Stretched Grids

The basic idea common to these approaches is that the element size is a function of space.

In the stretched grid, the size changes smoothly and is "mapped" onto a constant element size using a transformation. Examples include Butler and Sheng (6) and Birchfield (2).

Telescoping grids change the element size suddenly. An example of a telescoping grid using three sizes of elements is given by Greenberg (16). The solution between the grids is coupled in time, allowing waves to propagate across the grid interfaces.

Nested grids solve the system several times. They begin by using a coarse grid, and the resulting solution is used to provide the boundary condition for a smaller "nested", fine scale grid which lies within the large grid. The method does not allow "feedback" from this "nested" grid to the large grid. The earliest example of such an approach is Reid and Bodine (27).

The advantages of these approaches are: 1) the open boundary is moved far away from the area of primary interest thus minimizing the influence of assumptions made at the boundary, and 2) the boundary can be moved to a

region where more reasonable assumptions can be made. Computational costs are minimized by using a larger element size in regions of less interest, or smaller gradients.

There are a number of problems with this approach besides the obvious inelegance and increase in computational cost. For instance, the technique will numerically distort waves as shown by Lewis et al. (20), and Browning et al. (4). In addition the nested grid does not influence the external one, and this is not realistic in general.

Energy Absorbing Elements

The basic idea in this approach is to dissipate wave energy when it hits the ocean boundary. This has been done in a number of ways. Busby and Timpson (5) added elements to the outer perimeter of their grid, and they specified large damping coefficients in these elements. These elements are the numerical analogue to "horse hair mats" used in laboratory wave tanks.

The approach is conceptually simple and easy to set up. However, it has a number of disadvantages in that it:

- requires extensive iteration in selecting the model damping parameters. It is not obvious a priori which parameters will minimize reflection and maximize energy absorption;
- is computationally expensive for the study of long wave phenomena because many damping elements will have to be added in order to get effective damping;
- distorts waves running tangentially to the boundary; and
- generates an artificial alongshore pressure gradient for the case of cross-shelf boundaries in the presence of wind forcing. This occurs because the alongshore Ekman transport will encounter undirectional resistance.

Sommerfeld Condition

This approach runs a close second in popularity behind the variable specification technique. The Sommerfeld condition can be written as:

$$\frac{\partial \phi}{\partial t} + c \frac{\partial \phi}{\partial x} = 0 \quad [1]$$

where ϕ is either U or η , c is the wave celerity, and the x direction is assumed normal to the boundary.

The Sommerfeld condition is the proper boundary condition for freely propagating waves at a boundary with infinite extent. Free waves are governed by the wave equation - a hyperbolic equation. The primitive barotropic equations in their full form lie somewhere between hyperbolic and parabolic, but degenerate into the wave equation in the absence of rotation, wind forcing and viscous effects. If these terms are neglected then the Sommerfeld condition does apply to the primitive equations.

An alternative form of the Sommerfield condition has often been used with primitive equation models:

$$U = c \eta + K \quad [2]$$

The equation can be derived by writing the Sommerfield condition for both U and η , then using the continuity equation to derive two differential equations - one in space and the other in time. The solution to the two equations is of the form [2]. The constant, k , is usually taken as zero based on physical arguments.

The value for c in [1] and [2] must be determined, and in general this requires knowledge of the dispersion relationship for the waves in question. Unfortunately, the relationship is not generally known. Orlanski (24), Camerlengo and O'Brien (7), and Miller and Thorpe (22) suggest methods to calculate c using one-sided differencing methods. However, for homogeneous fluids the value for c is generally taken as the shallow water wave speed, \sqrt{gH} , where H is the local water depth. This of course neglects rotational effects.

Vastano and Reid (40,41) used [1] in the study of tsunami response. They found that the technique was limited by the fact that [1] only radiates waves which hit the boundary at a normal angle - oblique waves will be partially reflected. Mungall and Reid (23) present a modification of [1] which allows radially spreading waves to scatter outward through a rectangularly bounded basin. Additional studies by Hebenstreit et al. (18) show the methods gives satisfactory results.

Reid and Bodine (27) appear to be the first to have used [2]. They studied the free wave propagation of storm surge in Galveston Bay. Wurtele et al. (42) used [2] to compare with the results from Vastano and Reid (40,41). Wurtele et al. (42) looked at the 2-D problem in a rectangular grid, and used the normal component of velocity at an internal grid to calculate η on the boundary. They found only weak reflections and no instabilities.

The obvious advantage of these radiation conditions is that they will allow free waves to propagate out of the model boundaries much as they would in the real world. Previous work clearly indicates that the conditions can be successfully used in the study of many practical free wave problems such as tsunamis.

The technique has some limitations in that it cannot include nonlinearities, rotation, or forced waves.

The last limitation is clearly indicated in the theoretical foundations of the Sommerfield condition; yet many investigators have ignored this fact. For example, Heaps (17) used [2] in the study of wind-driven surge in the Irish Sea. Similarly, Blumberg and Kantha (3) used a form of [1] to study wind-driven synoptic currents on the Eastern U.S. continental shelf.

Application of [1] or [2] to the forced wave problem is not theoretically justified, and can lead to substantial errors particularly in the case of quasi-steady or steady flow. The condition [1] or [2] requires that a pressure gradient be set up in order for flow through the boundary to exist. In the case of wind-driven flow it is clear that flow can occur through the boundary in the

absence of a pressure gradient. Thus when [1] or [2] is used in wind-forced problems, an artificial pressure gradient is established.

The errors which results when [1] or [2] is used for the forced wave problem are illustrated in Figure 3. The figure shows the velocity profiles in an infinitely long channel of constant depth with a constant wind stress. Two different types of models are shown. The linear profile denoted by "Galerkin" is the steady-state result for a constant eddy viscosity model. It can be generated using the Galerkin model by specifying $\eta=0$ or $d\eta/dx=0$ at the downwind boundary. The dashed profile denoted by "Galerkin w. rad." is the velocity profile using a radiation boundary condition. Note the velocity has been decreased by roughly a factor of two. This is caused by the artificial pressure gradient generated by the radiation condition. A similar result is found for the vertically averaged model, also illustrated in the figure.

Forced/Free Wave Solution

As was pointed out above, the Sommerfield radiation condition is not really appropriate for the study of wind-driven or forced flow. In an effort to remove the forced restriction, Røed and Smedstad (28) developed a method which separates the primitive barotropic equations into two modes: a local or forced mode, and a global or free mode. Using a specialized topography illustrated in Figure 4, Røed and Smedstad (28) were able to eliminate the need for any boundary conditions for the local solution. The boundary condition for the global solution is [1].

The modal approach is theoretically attractive. However, a number of major assumptions regarding topography were made by (28). It remains to be seen whether the technique can be applied to the more general case.

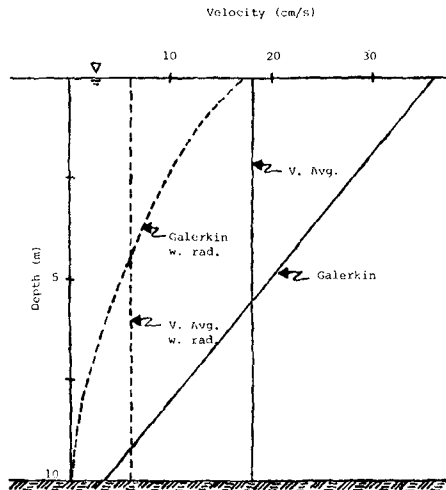


Figure 3: Comparison of profiles from two types of models using different downstream boundary conditions.

REVISED GRID SYSTEM RESULTS

All of the techniques identified in the previous chapter were considered for this study. Most would have required extensive program recoding or expansion of the existing grid system. The costs associated with these changes could not be justified given the preliminary nature of the study.

A compromise was developed which could be quickly implemented. It consisted of adding 10 columns to the western boundary of the grid shown in Figure 1 resulting in a 30 x 30 grid. No wind stress was imposed on these additional elements, and dissipation parameters in the elements were increased. In addition a radiation condition in the form of [2] was implemented in the model code along the western boundary.

On the lateral boundary, dn/dx was set to zero as in the initial grid. Adding additional rows on the cross-shelf boundaries as was done on the western boundary would have generated an artificial alongshore pressure gradient for reasons cited in the previous section. Seiching tendencies in the alongshore direction were minimized by eliminating the alongshore bathymetric gradients. This is not unreasonable for this section of the coast.

The model was run using the same forcing as in the initial run (see the third section above). Figure 5 shows representative results using the same empirical coefficients as in the initial run. Comparing this figure to Figure 2 indicates that the radiation condition does substantially reduce the seiche. As indicated in Figure 6, further reduction is achieved by increasing the vertical eddy viscosity and bottom friction by an order of magnitude in the western 10 columns. The figure should be compared to 2 to see the substantial improvement obtained with the revised boundary conditions.

HINDCAST RESULTS

Once the seiche was removed from the model, it was used to hindcast an actual storm event. Data was available for a major storm which occurred in late October 1974. Cardone (8) provided synoptic wind and pressure fields for the storm at six hour intervals. He used post-synoptic techniques, with data based on land, buoy, and ship data, as well as surface weather maps.

Figure 7 shows the wind vectors hindcasted by (8) near Bergen, on the Norwegian coast. Peak winds reached roughly 20 m/s. Wind direction was primarily from the north, shifting from northeast to northwest during the course of the storm. Spatial wind gradients were generally not large over the scale of the model grid.

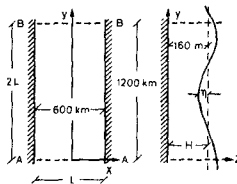


Figure 4: Topography of basin used in the free/forced wave boundary condition studies of Roed and Smedstad

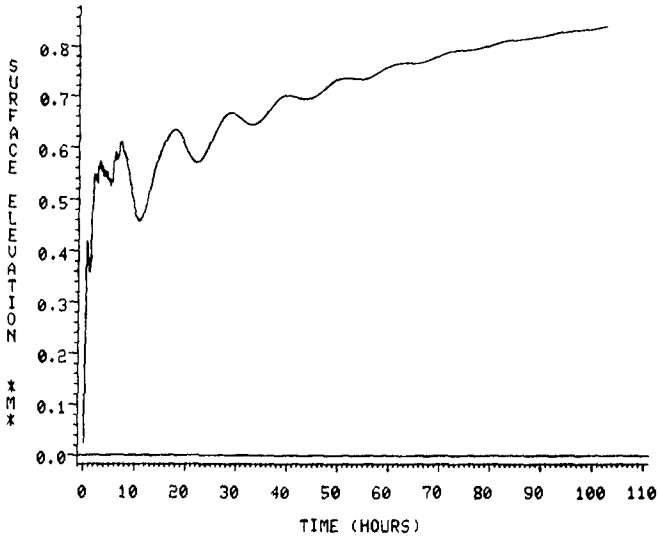


Figure 5: Modeled time series of surface elevation at the coast. Model grid is the same as Figure 2 except five additional columns have been added as well as a radiation boundary condition on western boundary.

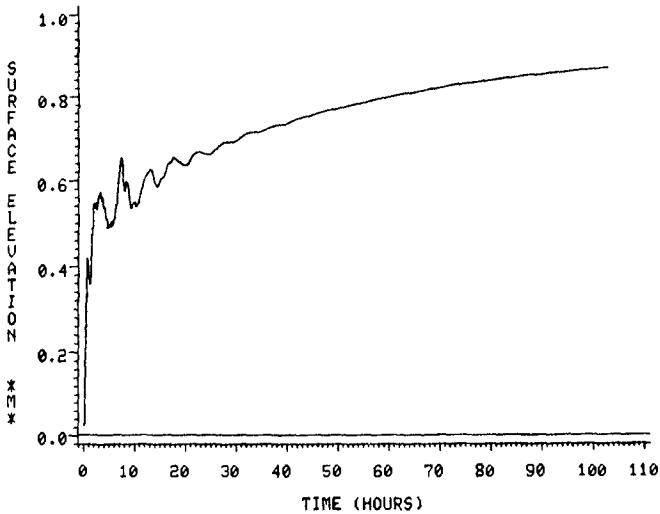


Figure 6: Modeled time series of surface elevation at the coast. Model grid is identical to Figure 5 except five outer columns have been made highly viscous.

The wind and pressure fields were used to force the ocean current model. Everything else was the same as described in the previous section.

Figure 8 shows the comparison at station SN10 marked by the uppermost solid circle in Figure 1. The modeled results are shown as a dashed curve and the data as solid. Both data and model results are taken at 50 m below the still water level. The upper panel in the figure shows the alongshore component with positive indicating a northerly direction. The lower panel shows the cross-shelf component with positive indicating an easterly flow. Comparisons are also available at other depths and sites but these are qualitatively similar to Figure 8, and are not shown.

In general the model predicts the right order of magnitude of the current but there are clearly some major discrepancies. The model results are predominately in the wind direction, while the data are not obviously correlated with the wind. The results can not be substantially improved by varying the model parameters N_V , c_b , or N_H .

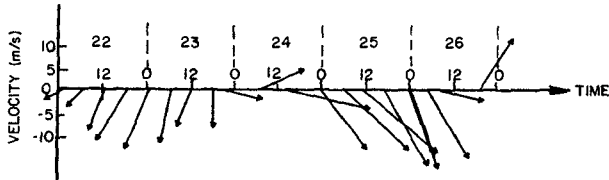


Figure 7: Time series of hindcasted wind vectors at the coast for the storm of October 1974.

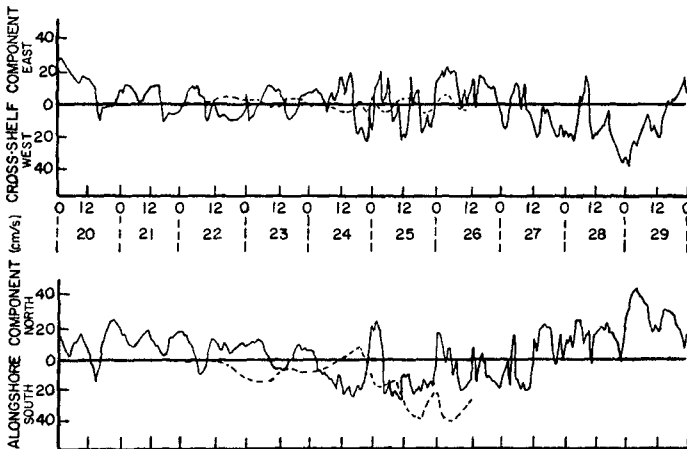


Figure 8: Comparison between modeled and observed currents at station SN10. Data is indicated by solid curve, and model by dashed curve.

The comparison is actually not as bad as it might first seem because the data still contain a relatively strong tidal signal, while the model contains no tidal forcing. An initial attempt was made to filter the tidal signal from the data, but this proved impossible using standard band-pass filters and least-squares or harmonic analysis. The reason for the difficulty is the nearly identical frequency of the inertial and tidal signal. One cannot apply any of these classical techniques without eliminating the inertial component, and of course this is not acceptable since a major portion of storm response of the shelf is inertial.

Figure 9 shows the modeled surface elevation at a central grid element on the coast. Two curves are shown. The dotted curve shows the result using the wind field provided by Cardone (8), whereas the solid curve used the same wind field but winds were updated every 30 minutes by interpolating the six-hour wind field. There are substantial differences between the two curves, indicating the dynamic sensitivity of the system. Much of this is due to the small role of friction in the basin.

Surge data had not been obtained at the time of this study for this particular storm. However, the magnitude of the modeled surge is consistent with other similarly severe storms (14).

SUMMARY AND CONCLUSIONS

The objective of the study was to make a first pass at modeling storm-driven currents and surge on the Southern Norwegian Shelf. A linear numerical model based on the barotropic primitive equations was used. Current data were available at several locations from some historical storms, and these were used to assess the model.

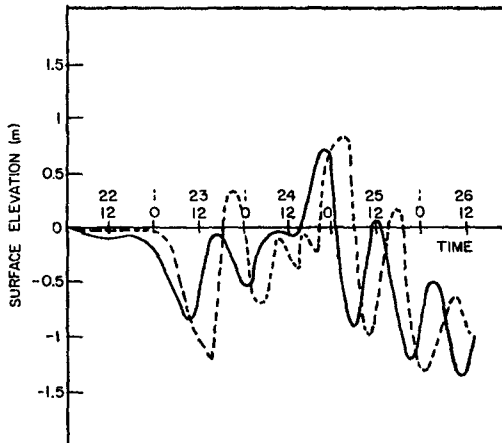


Figure 9: Time series of modeled surface elevation at the coast for storm of October 1974.

Friction was found to be of relatively little importance on the shelf, and storm response was strongly inertial. Stratification was generally negligible during the most severe storms, and hence the barotropic assumption was easily justified.

Preliminary application of the model to the shelf indicated the dominance of a seiche in the cross-shelf direction. The cause was traced to the reflective boundary conditions.

A fairly thorough review of the literature was undertaken in an attempt to find alternative boundary conditions which would eliminate the artificial seiche. Five types of conditions were identified, and examined. None of the conditions are universally applicable. One major finding is that many previous applications have used a radiation condition to study quasi-steady forced flow fields, and it is easily shown that this can generate substantial errors.

Eventually a boundary condition was found which eliminated the seiche. The configuration consisted of: 1) a highly viscous, unforced, outer western boundary, 2) a radiation boundary condition on the western boundary and 3) a simplified bottom bathymetry which eliminated alongshore oscillations.

Finally, the model was applied to hindcast currents during a major storm on the shelf. Results indicated the model gives the proper order of magnitude for both currents and surges. A more quantitative assessment was impossible because the data contained a strong tidal component which could neither be removed nor easily modeled.

Efforts are underway to improve the results described above. These improvements will include: 1) implementation of an improved boundary condition on all ocean boundaries, 2) expansion of the grid system to include the entire Norwegian Sea, 3) further data analysis to remove the tidal signal, or if this is not possible then tidal forcing will be included in the model, and 4) extension of the wind hindcasts to provide adequate model spin up.

REFERENCES

- ¹Beardsley, R. C. and D. B. Haidvogel, "Model Studies of the Wind-Driven Transient Circulation in the Middle Atlantic Bight. Part 1: Adiabatic Boundary Conditions," *J. Phys. Oceanogr.*, 11, 3, 355-375, 1981.
- ²Birchfield, G. E., "Numerical Prediction of Hurricane Movement with the Use of a Fine Grid," *J. Meteorol.*, 17, 406-414, 1960.
- ³Blumberg, A. F. and L. H. Kantha, "An Open Boundary Condition for Circulation Models," *J. Hydraulics*, ASCE, in press.
- ⁴Browning, G., H. O. Dreiss, and J. Olinger, "Mesh Refinement", *Math. Comp.*, 27, 29-39, 1973.
- ⁵Busby, F. H., and M. S. Timpson, *Quart. J. Roy Meteor. Soc.*, 93, 1, 1967.
- ⁶Butler, H. L. and Y. P. Sheng, "A Wave Separation/Radiation Boundary Condition for Limited Area Modeling of Coastal Project Impact," *Proc. 19th Inter. Conf. on Coastal Engng.*, Houston, ASCE, 1984.

- ⁷Camerlengo, A. L., and J. J. O'Brien, "Open Boundary Conditions in Rotating Fluids," *J. Comp. Phys.*, 35, 1, 12-35, 1980.
- ⁸Cardone, V., "Hindcast of North Sea Wind and Pressure Fields for Ocean Current Technology Project. Report submitted to Conoco, March 1982.
- ⁹Cooper, C. K. and B. R. Pearce, "Numerical Simulations of Hurricane-Generated Currents," *J. Phys. Oceanogr.*, 12, 1070-1091, 1982.
- ¹⁰Cooper, C. K. and B. R. Pearce, "GAL: A 3-D Circulation Model," T. R., MIT Ralph M. Parsons Laboratory, 1977.
- ¹¹Davies, A. M., "Application of the Galerkin Method to the Formulation of a 3-D Nonlinear Hydrodynamic Numerical Sea Model," *Appl. Math. Model.*, 4, 245-256, 1979.
- ¹²Eide, L. I., "Evidence of a Topographically Trapped Vortex on the Norwegian Continental Shelf," *Deep-Sea Res.*, 26, 6A, 1979.
- ¹³Forristall, G. Z., R. C. Hamilton and V. J. Cardone, "Continental Shelf Currents in Tropical Storm Delia: Observations and Theory," *J. Phys. Oceanogr.*, 7, 532-546, 1977.
- ¹⁴Gjevik, B., and L. R. Røed, "Storm Surges Along the Western Coast of Norway," *Tellus*, 28, 2, 166-182, 1976.
- ¹⁵Graham, C., "Strong Surface Currents at the Troll Field in the Norwegian North Sea," *Proceedings of Workshop on Joint Probability, E&P Forum, London, 1983.*
- ¹⁶Greenberg, D. A., "Modeling the Mean Barotropic Circulation in the Bay of Fundy and Gulf of Maine," *J. Phys. Oceanogr.*, 13, 5, 886-904, 1983.
- ¹⁷Heaps, N. S., "Development of a Three-Dimensional Numerical Model of the Irish Sea," *Rapp. P.-v. Reun., Cons. in. Explor. Mer.*, 167, 146-162, 1974.
- ¹⁸Hebenstreit, G. T., E. N. Bernard, and A. C. Vastano, "Application of Improved Numerical Techniques to the Tsunami Response of Island Systems," *J. Phys. Oceanogr.*, 10, 1134-1140, 1980.
- ¹⁹Lamb, H., *Hydrodynamics*, 6th edition, Dover Press, London, 1945.
- ²⁰Lewis, J. K., R. E. Whitaker, and W. J. Merrell, Jr., "The Effects of Stretched-Grid Coordinate System on Long-Wave Dispersion and Energy Characteristics," *J. Geophys. Res.*, 87, C6, 4265-4267, 1982.
- ²¹Lilly, D. K., "On the Computational Stability of Numerical Solutions of Time-Dependent Non-Linear Geophysical Fluid Dynamic Problems," *Monthly Weather Review*, 93, 1, 11-26, 1965.
- ²²Miller, M. J. and A. J. Thorpe, "Radiation Conditions for the Lateral Boundaries of Limited-Area Numerical Models," *Quart. J. R. Met. Soc.*, 107, 615-628, 1981.
- ²³Mungall, J. C. H., and R. O. Reid, "A Radiation Condition for Radially - Spreading Non-Dispersive Gravity Waves," TR 78-2-T, Dept. of Oceanography, Texas A&M, 63 pp., 1978.

- ²⁴Orlanski, I., "A Simple Boundary Condition for Unbounded Hyperbolic Flows," *J. Comp. Phys.*, 21, 251-269, 1976.
- ²⁵Ramming, H. G. and Z. Kowalik, Numerical Modelling of Marine Hydrodynamics, Elsevier Scientific, New York, 1980.
- ²⁶Reid, R. O., "Comment on 'Three-Dimensional Structure of Storm-Generated Currents' by G. Z. Forristall," *J. Geophys. Res.*, 80, 9, 1184-1185, 1975.
- ²⁷Reid, R. O., and B. R. Bodine, "Numerical Model for Storm Surges in Galveston Bay," *ASCE, WW1*, 33-57, 1968.
- ²⁸Røed, L. P., and O. M. Smedstad, "Open Boundary Conditions for Forced Waves in a Rotating Fluid," *SIAM J. Sci. Stat. Comput.*, 5, 2, 1984.
- ²⁹Thompson, J. D., "The Coastal Upwelling Cycle on a Beta-Phase Hydrodynamics and Thermodynamics," TR 22, Dept. of Met., Florida State, Tallahassee, 140 pp., 1974.
- ³⁰Townsend, A. A., The Structure of Turbulent Flow, Cambridge Univ. Press, 429 pp., 1976.
- ⁴⁰Vastano, A. C., and R. O. Reid, "Tsunami Response at Wake Island: Comparison of the Hydraulic and Numerical Approaches," *J. Marine Res.*, 28, 3, 345-356, 1970.
- ⁴¹Vastano, A. C., and R. O. Reid, "Tsunami Response for Islands: Verification of a Numerical Procedure," *J. Marine Res.*, 25, 2, 129-139, 1967.
- ⁴²Wurtele, M. G., J. Paegle, and A. Sielecki, "The Use of Open Boundary Conditions with the Storm-Surge Equations," *Monthly Weather Review*, 99, 6, 537-544, 1971.